

Wei LI, Rong XIONG, 2021. A hybrid visual servo control method for simultaneously controlling a nonholonomic mobile and a manipulator. *Frontiers of Information Technology & Electronic Engineering*, 22(2):141-154. <https://doi.org/10.1631/FITEE.1900460>

A hybrid visual servo control method for simultaneously controlling a nonholonomic mobile and a manipulator

Key words: Mobile manipulation; Hybrid visual servo; Eye-in-hand; Global Jacobian; Kalman filter

Corresponding author: Rong XIONG

E-mail: rxiong@zju.edu.cn

 ORCID: <https://orcid.org/0000-0001-9318-9014>

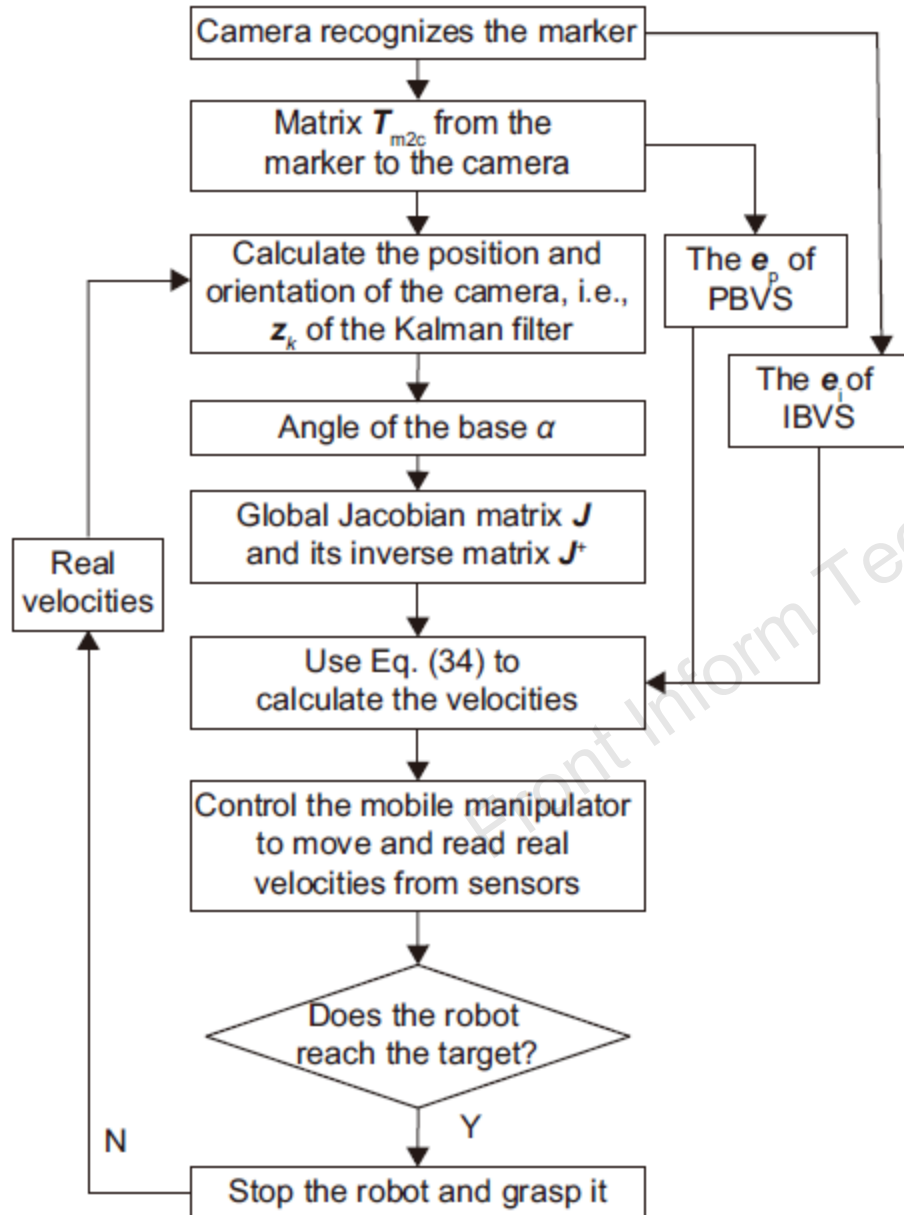
Motivation

At present, most visual servo control algorithms used in mobile manipulation separate the motion of the mobile bases and robotic arms. That means, the mobile bases are driven to the designated positions first, and then the robotic arms complete their tasks with the aid of camera vision. To improve the smoothness of the mobile manipulation process and save the operation time, in this study we try to find a visual servo method to control the arm and chassis as a whole; i.e., the robot can grasp while walking.

Main idea

1. Based on the differential kinematic equations of the mobile manipulator, the global Jacobian matrix of any point is derived when the mobile base moves on a 2D plane or in a 3D space.
2. Based on the analysis of the advantages and disadvantages of traditional image-based visual servo and position-based visual servo, a new hybrid visual servo method for mobile manipulation is proposed.
3. A new velocity control rule for mobile manipulation is derived by combining the hybrid visual servo method with the global Jacobian matrix. By using the velocity control rule that is integrated with the Kalman filter, the mobile manipulator can grasp while walking.

Method



$$J = \begin{bmatrix} & & T_1 & T_2 \\ & & T_3 & T_4 \\ R & \mathbf{0}_{3 \times 3} & 0 & 0 \\ \mathbf{0}_{3 \times 3} & R & 0 & 0 \\ & & 0 & 0 \\ & & 1 & 0 \end{bmatrix} \quad (16)$$

$$= \begin{bmatrix} J_{0(6 \times 6)} & \mathbf{0}_{6 \times 2} \\ \mathbf{0}_{2 \times 6} & I_{2 \times 2} \\ R \cdot J_{0t} & 0 & 0 \\ R \cdot J_{0r} & 0 & 0 \\ & 0 & 0 \\ & 1 & 0 \end{bmatrix}$$

$$\left[\frac{d\theta_1}{dt} \quad \frac{d\theta_2}{dt} \quad \frac{d\theta_3}{dt} \quad \frac{d\theta_4}{dt} \quad \frac{d\theta_5}{dt} \quad \frac{d\theta_6}{dt} \quad \omega \quad v \right]^T = -J^+(\kappa L_p^{-1} e_p + \lambda H L_i^+ e_i). \quad (34)$$

Results

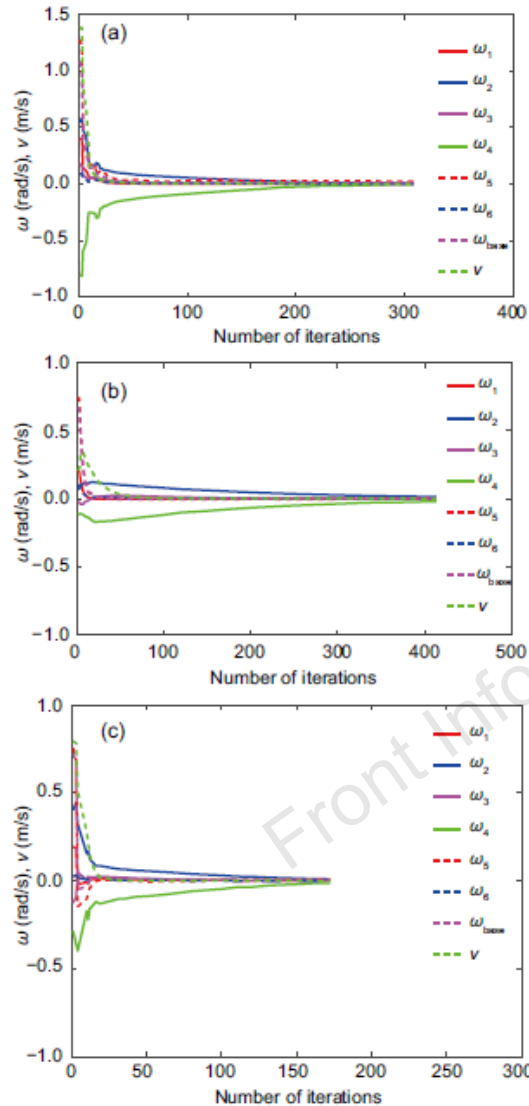


Fig. 5 Angular velocity or velocity of each degree of freedom of the robot as a function of time: planning results of the IBVS (a), PBVS (b), and HVS (c) algorithms

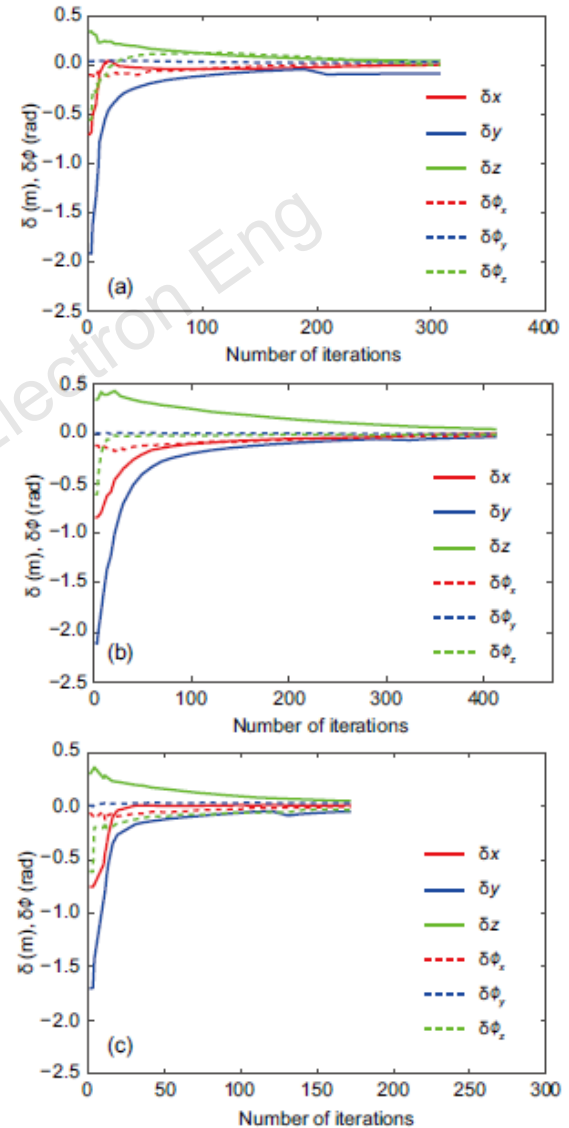


Fig. 6 Distance between the gripper and the target positions as a function of time: planning results of the IBVS (a), PBVS (b), and HVS (c) algorithms

Comparison

Table 1 Comparison of parameters of the three algorithms

Item	IBVS	PBVS	HVS
Displacement of the base (m)	1.8348	2.0020	1.7567
Distance of the base (m)	2.3442	2.3524	2.1396
Ratio of the actual path distance to the displacement of the base	1.2776	1.1750	1.2180
Displacement of the gripper (m)	1.9954	2.2932	1.8825
Distance of the gripper (m)	2.2313	2.4408	2.0566
Ratio of the actual path distance to the displacement of the gripper	1.1182	1.0644	1.0925
Time spent (s)	31	41	17.5
Largest velocity (m/s)	1.39	0.35	0.8

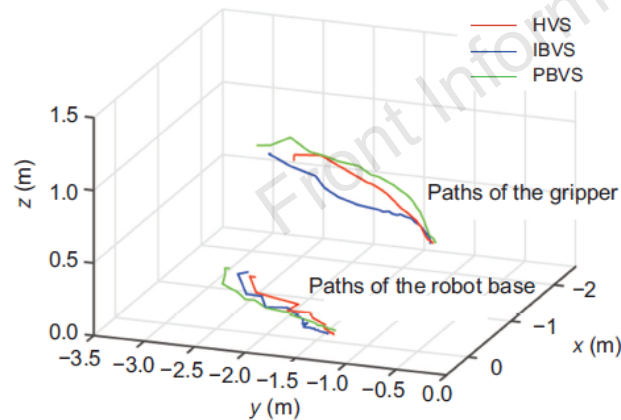


Fig. 4 Motion paths of the robot chassis and gripper in the real space of the three algorithms. References to color refer to the online version of this figure

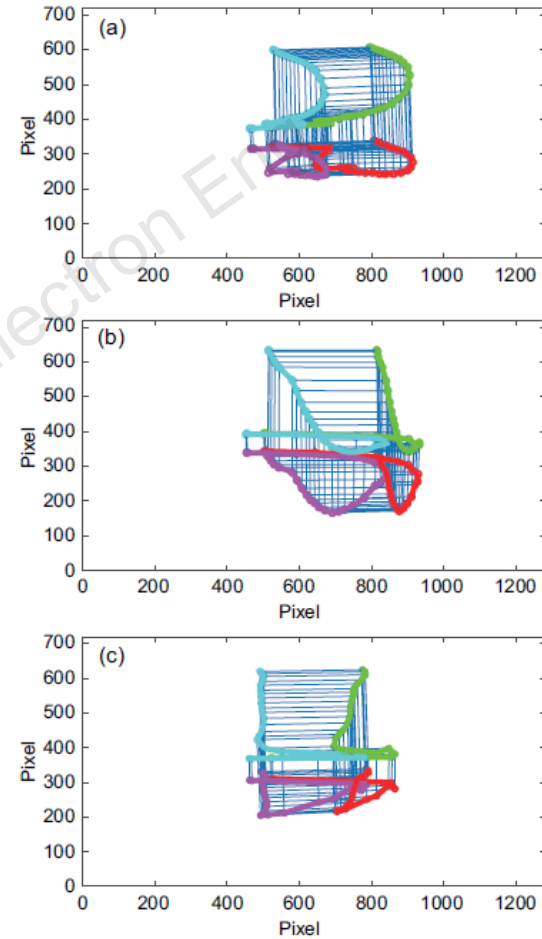


Fig. 7 Changes of positions of the four feature points on the camera image with time when the IBVS (a), PBVS (b), and HVS (c) algorithms are running, respectively

Kalman filter

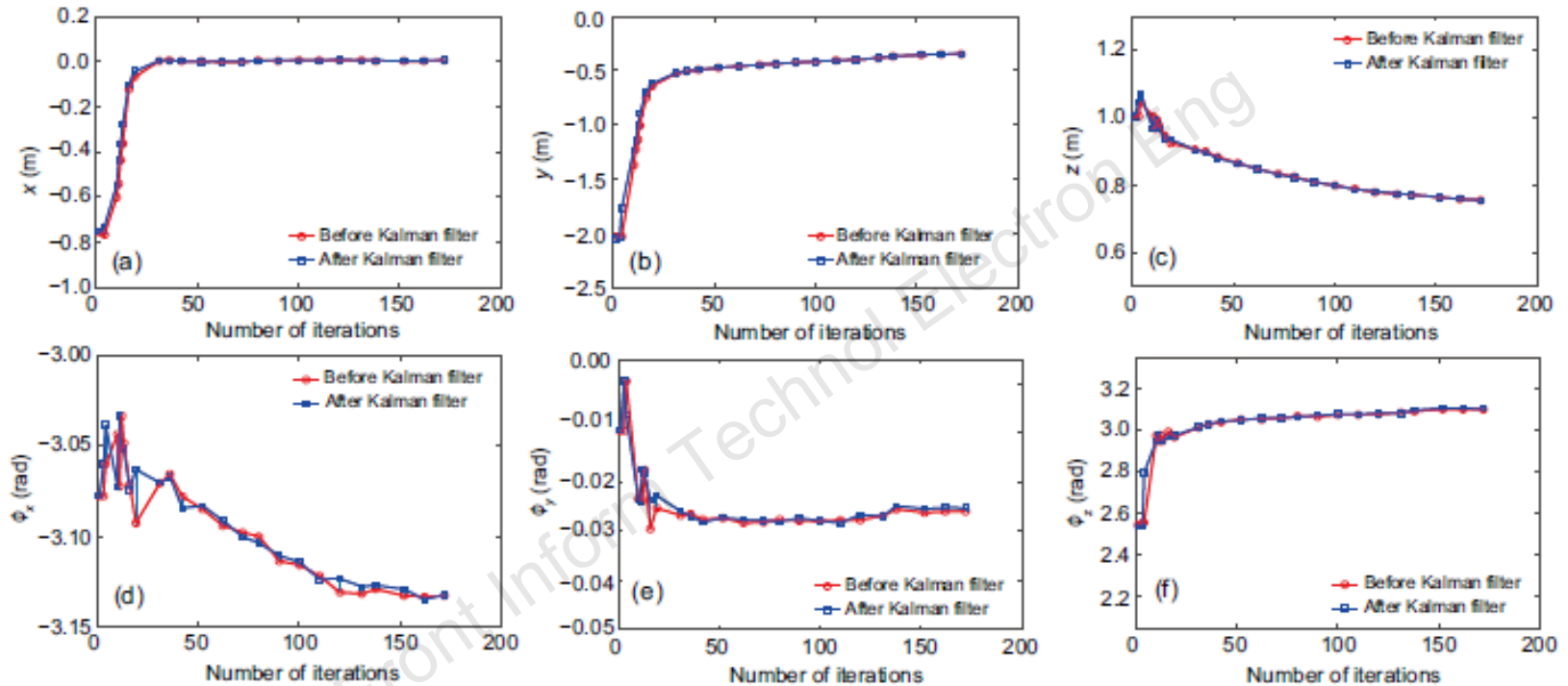


Fig. 8 Time-varying graph of pose data of the robot end gripper in the world coordinate system before and after using the Kalman filter: (a) end clamp data before and after filtering at the x -axis position; (b) end clamp data before and after filtering at the y -axis position; (c) end clamp data before and after filtering at the z -axis position; (d) end clamp data of the rotation angle before and after filtering in the x -axis direction; (e) end clamp data of the rotation angle before and after filtering in the y -axis direction; (f) end clamp data of the rotation angle before and after filtering in the z -axis direction

Verification

When the program is running, the robotic base and the arm move toward the marker at the same time. At the beginning, the base moves very fast (at about 0.8 m/s) and the robotic arm moves very slowly. However, when the gripper is close to the target bottle (<30 cm), the movement of the base becomes very slow (<1 cm/s), and the movement of the gripper toward the target is caused mainly by the robotic arm.



Fig. 9 Verification of the HVS method using a real robot

Outlooks

1. By further optimizing the conditions of visual servo, the target visual marker can be removed, the target object can be directly observed, or the convolutional neural network can be used to generate the bounding box as its visual marker for servo.
2. Further optimize the last trajectory to speed up the whole visual servo process.
3. A global visual servo with a repulsive field of obstacles can be added.



Wei LI received the MS degree from University of Science and Technology of China in 2013, and received the Ph.D. degree from Zhejiang University in 2020. His research interests include mobile manipulation and order picking.



Rong XIONG received the BS and MS degrees in Computer Science and Engineering, and the PhD degree in Control Science and Engineering from Zhejiang University, Hangzhou, China, in 1994, 1997, and 2009, respectively. She is currently a professor at the College of Control Science and Engineering, Zhejiang University. Her research interests include intelligent perception and control for mobile robots and manipulators.